Laboratory Flushing Tests of Dissolved Contaminants in Heterogeneous Porous Media with Low-Conductivity Zones

Kurasawa, Tomoki

Takahashi, Yoshitaro

Suzuki, Mariko

Inoue, Kazuya

(Citation)
Water, Air, & Soil Pollution,234(4):240

(Issue Date)
2023-04

(Resource Type)
journal article

(Version)
Version of Record

Water Air Soil Pollut (2023) 234:240
https://doi.org/10.1007/s11270-023-06236-5

Laboratory Flushing Tests of Dissolved Contaminants in Heterogeneous Porous Media with Low-Conductivity Zones

Tomoki Kurasawa · Yoshitaro Takahashi · Mariko Suzuki · Kazuya Inoue

Received: 16 November 2022 / Accepted: 13 March 2023 / Published online: 29 March 2023

Abstract The retention of contaminants within low-conductivity regions such as clay lenses and aquitards can greatly affect groundwater remediation processes. The aim of this study was to experimentally investigate the effects of the geometry of low-conductivity zones, conductivity contrast, and flow regime on solute flushing. We conducted a series of flushing tests in cylindrical models containing a cylindrical low-conductivity zone (i.e., low-*K* zone) embedded in a highly conductive medium (i.e., high-*K* zone). Seven models comprising four high-conductivity-contrast (SL, SS, LL, and LS), one medium-contrast (LLM), one low-contrast (LLL), and one homogeneous (H) models were considered. Experiments were conducted at two flow rates ($Q = 0.6$ and 26 cm^3/min) for each heterogeneous model (SL, SS, LL, LS, LLM, and LLL) to compare the flushing processes in different flow regimes. First, we verified the validity of our experiments by comparing the results of the H model from an analytical solution with our experiment. The results of the high-contrast models showed that for a diffusion-dominated regime ($Q = 0.6$ cm^3/min), the pore volume injected (PVI) required to flush out solute mass was much smaller than that in an advection-dominated regime ($Q = 26$ cm^3/min). To evaluate the pore volumes required to flush out solutes for the four high-contrast models, we introduced a parameter $P_{0.01}$, which is defined as the PVI needed for the relative concentration to become 0.01 at the middle of the low-*K* zone. $P_{0.01}$ decreases with increasing the specific surface area of the low-*K* zone for diffusion-dominated regimes, while it increases with increasing the length of the low-*K* zone for advection-dominated regimes. We also determined the importance of the effect of *K* contrast on solute retention by comparing the results of three different models of *K* contrast (LL, LLM, and LLL).

Keywords Flushing test · Solute contaminant · Heterogeneous porous media · Low-conductivity zone · Back diffusion · Advection

1 Introduction

Pump and treat (P&T) is a commonly used method for the remediation of groundwater contaminated with dissolved chemicals (United States Environmental Protection Agency, 2020). The P&T procedure is based on a simple principle: contaminated groundwater is extracted from the aquifer using wells or trenches and then sent to specific treatment plants to reduce pollutant concentrations.

T. Kurasawa
Graduate School of Agriculture, Ehime University, 3-5-7 Tarumi, 7908566 Matsuyama, Ehime, Japan

Y. Takahashi · M. Suzuki · K. Inoue (✉)
Graduate School of Agricultural Science, Kobe University, 1-1 Rokkodai, Nada-Ku, Kobe 6578501, Japan
e-mail: mornel@kobe-u.ac.jp

However, when the aquifer contains low-conductivity (*K*) zones (e.g., silty or clayey layers or lenses and aquitards), the effectiveness of flushing by P&T technology will be limited. Once a contaminant enters low-*K* zones, it persists for an extremely long period. If the flow velocity is extremely low in these zones (and thus, the contribution of molecular diffusion is not neglected), these zones release the contaminant via molecular diffusion and advection. The release of the contaminant via diffusion is called back diffusion (Brooks et al., 2020; You et al., 2020).

It is important to study back diffusion from low-*K* zones because this phenomenon is responsible for the long-term tailing of a contaminant plume. Therefore, improving our understanding of back diffusion has garnered considerable interest over the past few decades. Parker et al. (2004) and Chapman and Parker (2005) investigated the tailing of the TCE plume because of back diffusion in a contaminated area in an industrial facility. Brusseau and Guo (2014) analyzed the concentration data obtained through remediation processes using P&T technology for five selected sites to investigate the plume-persistence characteristics and reported that back diffusion is a key factor for removing contaminants. Moreover, Blue et al. (2023) reviewed available literature on the remediation of plume persistence due to back diffusion and conducted case studies for four selected sites. However, as it is difficult to capture the complexities of contaminant plume migration on the field, numerical simulations and controlled laboratory experiments have been useful tools in the studies on the fundamental process of plume migration. Parker et al. (2008) numerically evaluated the effects of back diffusion on a sand aquifer in Florida. Chapman et al. (2012) validated the use of numerical models, such as HydroGeoSphere, FEFLOW, and MODFLOW/MT3DMS, to simulate diffusion into and out of low-*K* zones. They conducted a laboratory experiment that served as a benchmark for validating numerical codes. In addition, visualization techniques, which have been widely used for understanding contaminant hydrogeological processes (Abdoulhalik & Ahmed, 2017; Castro-Alcalá et al., 2012; Citarella et al., 2015; Jaeger et al., 2009; Kurasawa et al., 2020, 2022; McNeil et al., 2006), have been applied to evaluate back diffusion (Tatti et al., 2016, 2018; Yang et al., 2014, 2019). Moreover, Tatti et al. (2019) performed both experimental and numerical investigations to demonstrate the suitability of a groundwater recirculation well (GCW) system to restore contaminated low-*K* zones as an alternative remediation technology to the traditional P&T.

Most of the aforementioned studies focused on evaluating back diffusion; however, few studies dealt with mass release via advection. Zinn et al. (2004) conducted laboratory experiments in heterogeneous media containing circular low-*K* zones and demonstrated that the media can produce a tailing effect driven by both diffusion and advection. Guswa and Freyberg (2000) investigated plume tailing in heterogeneous media with an elliptical low-*K* lens by adopting random walk particle tracking. They found that the transport regime (i.e., advection- or diffusion-dominant) within the lens remarkably affects plume tailing. Di Palma et al. (2017) performed pore-scale simulations to evaluate the effects of different transport mechanisms (i.e., advection or diffusion) on solute retention within a low-*K* zone and showed that when diffusion is dominant in the zone, the dimensionless time (i.e., the cumulative value of the flow) required to flush out the solute plume is smaller than that when advection is dominant; thus, molecular diffusion can facilitate efficient contaminant flushing within low-*K* zones. Di Palma et al. (2017) also found that solute retention depends on the geometry of the low-*K* zone and the *K* contrast between the high- and low-*K* zones. However, literature on systematic evaluations of the influence of such factors on solute retention is scarce; in particular, to the best of our knowledge, there has been no experimental investigation of such influence.

The main objective of this study was to experimentally investigate the effect of factors such as the geometry of low-*K* zones, *K* contrast, and flow regime, on solute flushing. We considered a cylinder model containing a cylindrical low-*K* zone embedded in a highly permeable medium. In all, 13 flushing tests were performed under different conditions using a laboratory column. Finally, we evaluated the effect of the aforementioned factors on solute flushing characteristics.

2 Materials and Methods

2.1 Model Porous Media

Our cylindrical model is shown in Fig. 1. It has a diameter of 10.8 cm and a height of 30 cm. A

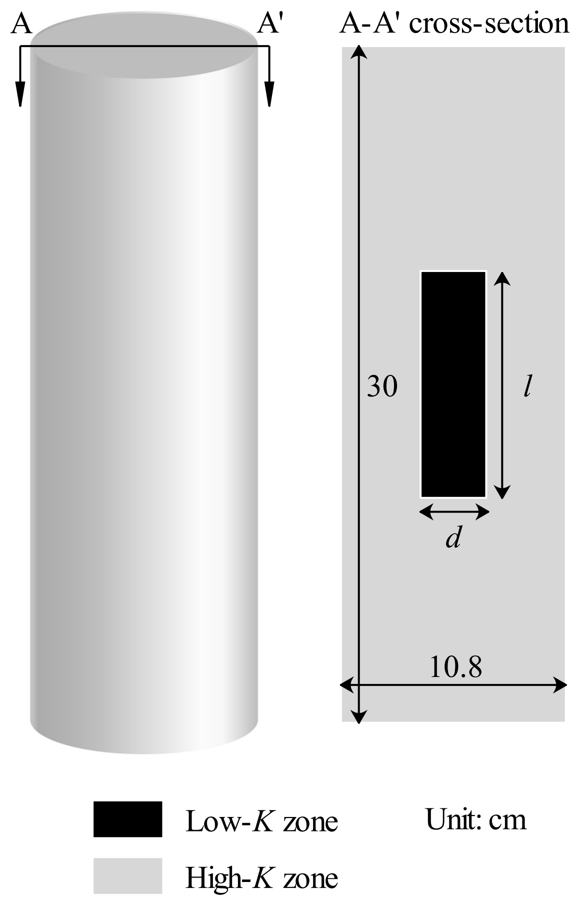

Fig. 1 Schematic of the investigated model with a diameter of 10.8 cm and a height of 30 cm; the model has a cylindrical low-K zone (i.e., low-conductivity zone) with diameter d and height l (both in centimeters)

cylindrical low-K zone with diameter d and height l (both in centimeters) is embedded in the middle of the model. The geometry of the low-K zone was varied by changing two variables, i.e., d and l. Thus, seven experimental models, which included a base model (i.e., homogeneous (H) model), were designed to investigate the solute flushing characteristics in response to the changes in the low-K zone geometry and K contrast (Table 1). The ratio of the hydraulic conductivity of a high-K zone to that of a low-K zone, K_{out}/K_{in}, is 94 for four high-contrast models (SL, SS, LL, and LS). The SL and SS models have the same volume of low-K-zones, but they differ in their geometry (i.e., d and l). The LL and LS models contain low-K zones of shapes similar to those of the SL and SS models, respectively. In addition, we considered different conductivity models, LLM ($K_{out}/K_{in} = 11$) and LLL ($K_{out}/K_{in} = 2$) that have low-K zones with shapes identical to the low-K zone of the LL model. The experimental process was validated by comparing the experimental result with the result of the H model obtained from an analytical solution described later in Section 3.1.

2.2 Experimental Setup

Flushing tests were performed in a cylindrical column with internal dimensions (height: 30 cm and diameter: 10.8 cm; see Fig. 2); we generated the cylindrical models shown in Fig. 1. A deionized water container and a container filled with NaCl solution (10 mg/cm^3) were connected to the bottom (i.e., the inlet) of the column through pumps that were used to maintain a constant flow rate during the experiments. Both containers were maintained at a constant temperature of 20 °C. The valves enabled immediate switchover between different fluid supplies (i.e., deionized water and NaCl solution) without interrupting the flow. The NaCl concentrations during the flushing tests were measured using an electrical conductivity sensor inserted in the middle of the column (i.e., in the middle of the low-K zone).

2.3 Experimental Procedure

The cylindrical models were constructed using four types of crushed silica sand, see Table 2. Specifically, the high-contrast (SL, SS, LL, and LS), medium-contrast (LLM) and low-contrast (LLL) models were created by combining sand types S1 and S4, S1 and S3, and S1 and S2, respectively. The homogeneous (H) model consisted of S4 only.

The column was packed layer-wise in a fully saturated condition to avoid trapping air and to achieve a porosity of 0.44. A narrow plastic divider was used to establish a sharp contact between the low- and high-K zones.

Figure 3 shows the experimental procedure of the flushing test. First, we continued to inject NaCl solution (10 mg/cm^3) into the column during more than twice the time required to reach a value of 10 mg/cm^3 (i.e., saturated condition) at the position of the sensor so that the porous medium was fully saturated with NaCl. After saturation, the valves were switched from NaCl solution to deionized

Table 1 Summary of experimental models

Schematic	Model	Abbrev.	Dimensions of low-K zone, d, l (cm)	Volume of low-K zone, V (cm^3)	Specific surface area of low K-zone, As (cm^2)	K contrast (−)	Porosity, θ (−)
	Homogeneous	(H)	–	–	–	–	0.44
	Small volume, Long zone	(SL)	2.0, 5.6	18	2.4	94	0.44
	Small volume, Short zone	(SS)	3.0, 2.5	18	2.1	94	0.44
	Large volume, Long zone	(LL)	4.0, 11.1	140	1.2	94	0.44
	Large volume, Short zone	(LS)	6.0, 5.0	140	1.1	94	0.44
	Large volume, Long zone, Medium contrast	(LLM)	4.0, 11.1	140	1.2	11	0.44
	Large volume, Long zone, Low contrast	(LLL)	4.0, 11.1	140	1.2	2	0.44

water ($t = 0$). Concentrations were then measured over time at the middle of the low-K zone. To evaluate the effects of the transport regime within the low-K zone on the solute flushing process, we performed experiments with two flow rates ($Q = 0.6$ and 26 cm^3/min) for each heterogeneous model (SL, SS, LL, LS, LLM, and LLL). However, the experiment for the H model was conducted only at a flow rate of 0.6 cm^3/min.

2.4 Estimation of the Flow Regime in the Low-K Zone

We employed the method of Zinn et al. (2004) to quantify the flow regime. They defined the Peclet number Pe (the ratio of the time scale of diffusion to the time scale of advection through a low-K zone) and the Damköhler number Da (the ratio of the time scale of advection across the whole cylindrical medium to the time scale of diffusion through the low-K zone). In this study, we defined these dimensionless numbers as follows:

$$Pe = \frac{v_{in} R^2}{l D_{ef}} \tag{1}$$

$$Da = \frac{L D_{ef}}{v_{out} R^2} \tag{2}$$

where R and l are the radius and length of the low-K zone, respectively; L is the length of the cylindrical column; $D_{ef} = \tau D$ is the effective diffusion coefficient of the porous media, where τ is the tortuosity and D is the aqueous diffusion coefficient. In our study, the tortuosity and aqueous diffusion coefficient were set as $\tau = 0.680$ (Bear, 1972), $D = 1.00 \times 10^{-9}$ m^2/s (Appelo & Postma, 2010). Additionally, v_{in} and v_{out} are the velocities in the low- and high-K zones, respectively. They were calculated using the flow rate

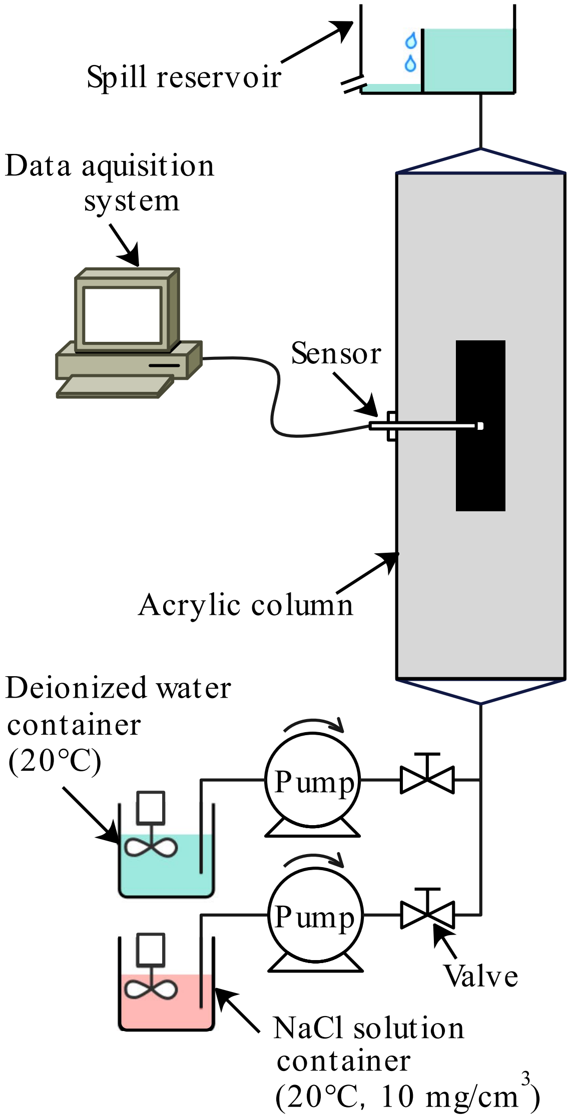

Fig. 2 Schematic of the experimental apparatus used to conduct flushing tests. The sensor was inserted into the middle of the column (middle of the low-K zone); the valves enabled an immediate switchover between the NaCl solution and deionized water

Table 2 Physical properties of four types of silica sand

	Grain size (cm)	Hydraulic conductivity (cm/s)	Porosity (-)
S1	0.140–0.200	0.450	0.44
S2	0.0425–0.0850	0.217	0.44
S3	0.0250–0.0425	0.0400	0.44
S4	0.0106–0.0250	0.00480	0.44

Q and ratio of the hydraulic conductivities of the low- and high-K zones (Zinn et al., 2004):

$$v_{in} = \frac{K_{in}}{K_{out}} \times \frac{Q}{A\theta} \tag{3}$$

$$v_{out} = \left(1 - \frac{K_{in}}{K_{out}}\right) \times \frac{Q}{A\theta} \tag{4}$$

where K_{in} and K_{out} are the hydraulic conductivities of the low- and high-K zones, respectively; Q is the flow rate; A is the cross-sectional area of the column; θ is the porosity.

When $Pe > Da^{-1}$ or $Da > 1$, limited tailing (i.e., a Fickian region) is expected. In contrast, tailing is pronounced if advection or diffusion in the low-K zone is much slower than advection in the high-K zone (i.e., $Pe < Da^{-1}$ and $Da < 1$). Specifically, for $Pe > 1$ and $Pe < Da^{-1}$, we expect an advection-dominated regime within the low-K zone, whereas for $Pe < 1$ and $Da < 1$, we expect a diffusion-dominated regime. Thus, when $Pe < Da^{-1}$ and $Da < 1$, the line of $Pe = 1$ represents the transition line between advection- and diffusion-dominated regimes.

Table 3 lists the calculation results of the flow regime for the experimental models. For the high-contrast models, the flow regime is diffusive mass transfer if the flow rate is small ($Q = 0.6$ cm^3/min), while it is advective mass transfer if the flow rate is large ($Q = 26$ cm^3/min). In contrast, medium-contrast (LLM) and low-contrast (LLL) models are within the advection and Fickian regions, respectively, for both low and high flow rate conditions.

3 Results and Discussion

3.1 Validation of the Experimental Process

For a homogeneous porous medium (H model), an analytical solution for the flushing test can be written as follows (Zinn et al., 2004):

$$\frac{C(x,t)}{C_0} = 1 - \frac{1}{2}\mathrm{erfc}\left(\frac{x}{2\sqrt{D_L t}}\right) \tag{5}$$

where C is the concentration; C_0 is the initial concentration; x is the longitudinal distance; t is time; and D_L is the longitudinal dispersion coefficient. Figure 4

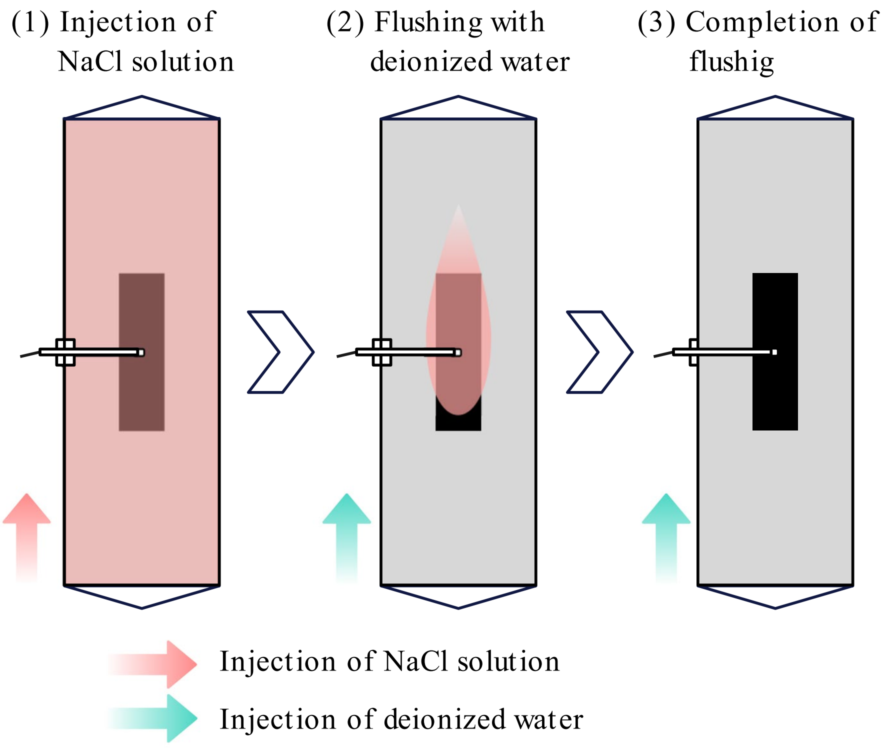

Fig. 3 Experimental procedure of the flushing test. The column was fully saturated with the NaCl solution (1) and subsequently flushed with deionized water (2) until the NaCl concentration became zero at the sensor position (3)

Table 3 Calculation results for different flow regimes

Model	Flow rate, Q (cm^3/min)	v_{in} (cm/s)	v_{out} (cm/s)	log Pe	log Da	Flow regime
SL	0.6	2.66×10^{-6}	2.47×10^{-4}	-1.16	-0.08	Diffusion
	26	1.16×10^{-4}	1.08×10^{-2}	0.49	-1.72	Advection
SS	0.6	2.66×10^{-6}	2.47×10^{-4}	-0.45	-0.44	Diffusion
	26	1.16×10^{-4}	1.08×10^{-2}	1.19	-2.08	Advection
LL	0.6	2.66×10^{-6}	2.47×10^{-4}	-0.85	-0.69	Diffusion
	26	1.16×10^{-4}	1.08×10^{-2}	0.79	-2.33	Advection
LS	0.6	2.66×10^{-6}	2.47×10^{-4}	-0.15	-1.04	Diffusion
	26	1.16×10^{-4}	1.08×10^{-2}	1.49	-2.68	Advection
LLM	0.6	2.22×10^{-5}	2.28×10^{-4}	0.07	-0.65	Advection
	26	9.71×10^{-4}	9.95×10^{-3}	1.71	-2.29	Advection
LLL	0.6	1.20×10^{-4}	1.29×10^{-4}	0.81	-0.40	Fickian
	26	5.26×10^{-3}	5.65×10^{-3}	2.45	-2.04	Fickian

shows the breakthrough curve for the H model; the curve was measured at the sensor positioned at the middle of the column. In addition, the figure shows the curve fitted by the analytical solution shown in Eq. (5). Breakthrough curves are expressed in terms of pore volume injected (PVI)—the fractional volume of the fluid injected relative to the total pore volume of pore space in a column. Thus, PVI represents dimensionless time.

The experimental data agreed well with the analytical solution. Furthermore, as expected, when PVI = 0.5, the relative concentration was approximately 0.5. From these results, we validated our experimental process.

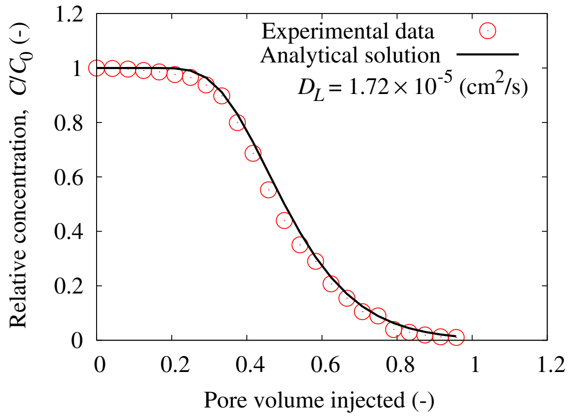

Fig. 4 Breakthrough curves for the H model shown as a function of the pore volume injected (PVI). The red circles represent the experimental results, and the solid line represents the fitting result of the analytical solution (Eq. 5)

3.2 Results of the High-Contrast Models

Figure 5 compares the breakthrough curves obtained from the high-contrast models (SL, SS, LL and LS). Compared with the H model (see Fig. 4), longer PVI was required to flush out the NaCl solution for heterogeneous models (Fig. 5), regardless of the flow rate. This emphasizes the importance of the effect of a low-K zone on solute flushing. On the other hand, for high-contrast models with a low flow rate ($Q = 0.6$ cm^3/min), less PVI was required to flush out the solute compared to the case with high flow rate ($Q = 26$ cm^3/min). Specifically, for the LL model, when $Q = 26$ cm^3/min, the relative concentration approached zero when considering a PVI of approximately 50, while when $Q = 0.6$ cm^3/min, PVI was approximately 9. This discrepancy is attributed to the difference in the flow regimes at high and low flow rates. Figure 6 presents the difference in flushing processes between advection- and diffusion-dominated regimes. As shown in this figure, for

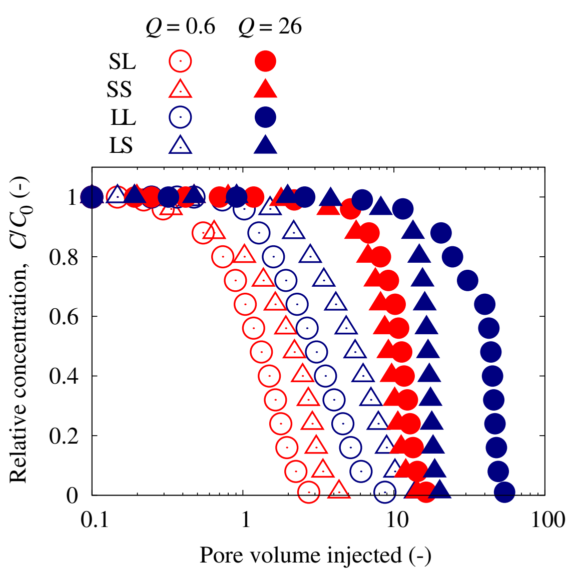

Fig. 5 Breakthrough curves for the high-contrast models (SL, SS, LL, and LS) shown as a function of the pore volume injected (PVI). The red and blue symbols represent the small- (SL and SS) and large-volume models (LL and LS), respectively, while the open and closed symbols represent the low- ($Q = 0.6$ cm^3/min) and high-flow-rate conditions ($Q = 26$ cm^3/min)

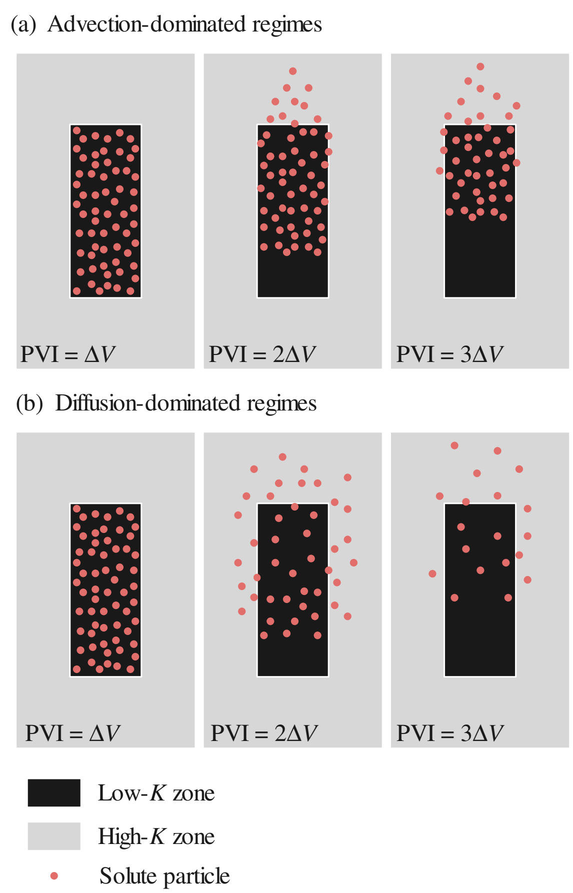

Fig. 6 Difference in the flushing processes between (**a**) advection- and (**b**) diffusion-dominated regimes. Here, to simplify the problem, we assumed that when PVI = ΔV, solute particles exist only in the low-K zone

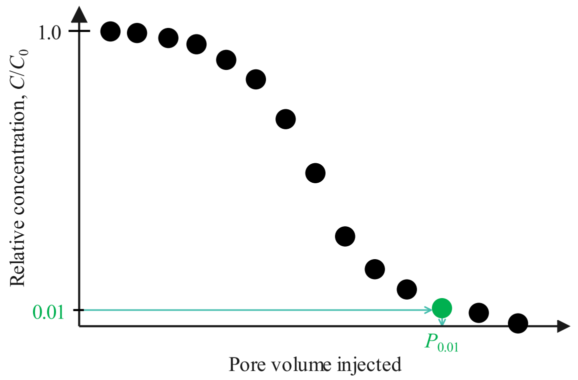

Fig. 7 Parameter $P_{0.01}$ defined as the PVI needed for the relative concentration to reach a value of 0.01 at the sensor position

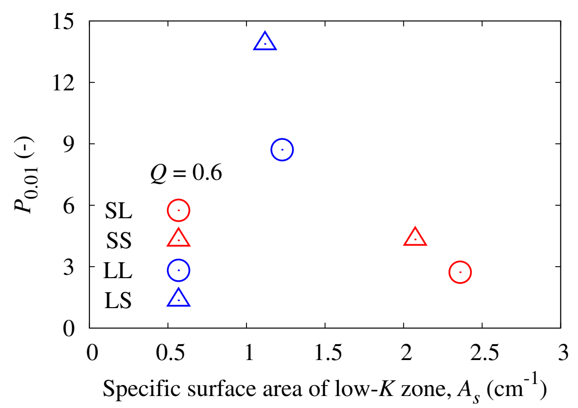

Fig. 8 $P_{0.01}$ for the diffusion-dominated regime as a function of the specific surface area of the low-K zone. The red circle and triangle represent the SL and SS models, respectively, while the blue circle and triangle represent the LL and LS models, respectively

advection-dominated regimes ($Q=26$ cm^3/min), the solute mass is released from the downstream face of the low-K zone via only advection, while for diffusion-dominated regimes, the solute is removed from all surfaces (including the sides and upstream and downstream faces) via diffusion and from the downstream face via slow advection. Therefore, in terms of the dimensionless time (i.e., PVI), the NaCl solution was flushed out quickly when diffusion was dominant ($Q=0.6$ cm^3/min). These results agree with the numerical simulation results of Di Palma et al. (2017) and provide insight into the influence and importance of flow velocity on the performance of the P&T process. Interestingly, in Fig. 5, for each model, the solute concentration in the advection-dominated regime exhibited a relatively sharp decrease than that in the diffusion-dominated regime. When advection was dominant, advection in the longitudinal direction pushed the solute mass out of the low-K zone, resulting in rapid decay of the solute concentration. In contrast, when diffusion was dominant, the solute slowly diffused out of the low-K zone, leading to a relatively slow decrease.

Furthermore, to evaluate the pore volume required to flush out the NaCl solution, we introduced a parameter $P_{0.01}$, which is defined as the PVI needed for the relative concentration to reach a value of 0.01 at the sensor position (i.e., the dimensionless time when the solute is nearly removed from the middle of the low-K zone). Figure 7 shows an illustration of $P_{0.01}$. As release from all surfaces of the low-K zone via diffusion contributes greatly to solute flushing for diffusion-dominated regimes, $P_{0.01}$ should depend on the specific surface area As of the low-K zone; As is defined as the total surface area per volume of the low-K zone. Therefore, in Fig. 8, we show the relationship between As and $P_{0.01}$ for the high-contrast models. As expected, the value of parameter $P_{0.01}$ decreases monotonically with increasing the specific surface area. On the other hand, in advection-dominated regimes, the solute was mainly removed from the downstream face via advection; hence, $P_{0.01}$ is regarded to depend on the length of the low-K zone. Figure 9 shows the relationship of $P_{0.01}$ with the length of the low-K zone in the direction of the flow. $P_{0.01}$ tends to increase with the length of the low-K zone. Finally, we emphasize that the specific surface area and length of the low-K zone are the key geometrical factors for diffusion- and advection-dominated regimes, respectively.

3.3 Effect of K Contrast

Figure 10 shows the breakthrough curves obtained from three different models of K contrast (LL, LLM, and LLL). Notably, for both low-contrast models (LLM and LLL), the breakthrough curves of $Q=0.6$ and $Q=26$ are very similar, suggesting that since LLM and LLL models are in the same regime, regardless of the flow conditions (see Table 3), the flow rate did

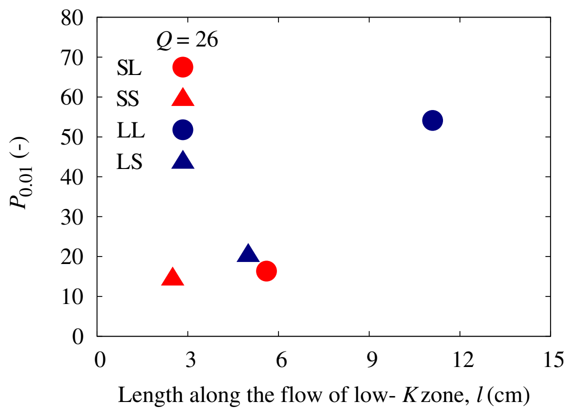

Fig. 9 $P_{0.01}$ for the advection-dominated regime as a function of the length of the low-K zone in the flow direction. The red circle and triangle represent the SL and SS models, respectively, while the blue circle and triangle represent the LL and LS models, respectively

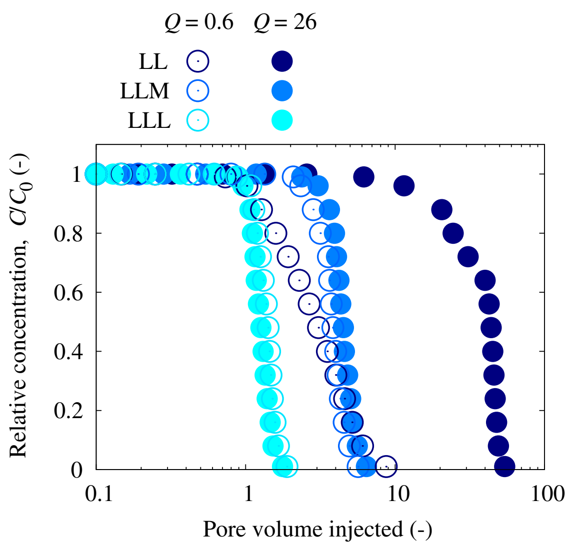

Fig. 10 Breakthrough curves for three different models of K contrast (LL, LLM, and LLL; shown as a function of PVI). The dark and light blue symbols represent the LL and LLL models, respectively, while the intermediate color symbols represent the LLM model. The open and closed symbols represent the low- ($Q = 0.6$ cm^3/min) and high-flow-rate conditions ($Q = 26$ cm^3/min)

not affect solute flushing. Meanwhile, there is a distinct difference between the PVI values required to flush out the NaCl solution for LLM and LLL models, indicating the importance of the effect of K contrast on solute flushing. Another interesting point is that for the LL model in the advection regime ($Q = 26$), the PVI needed for the relative concentration to approach zero is relatively large (more than 50), while in the diffusion regime ($Q = 0.6$), the corresponding PVI value is remarkably lower, resulting in the same order of magnitude as those obtained from the LLM model.

3.4 Comparison of the Flow Regimes Observed in our Experiments and Previous Works

To compare the flow regimes of our work with those of previous studies, the *Pe* and *Da* numbers determined in this study and previous experiments are plotted in Fig. 11. As we can see from this figure, a relatively large number of studies have explored the Fickian regime. Further, this work and the work of Zinn et al. (2004) only have the data that cover the three different regimes (Fickian, advection, and diffusion regions). Note that only our experiments show the transition from the diffusion regime to the advection regime in the same porous models (SL, SS, LL and LS models) achieved by drastically changing the flow rate.

4 Summary and Conclusions

In this study, we conducted a series of experiments focused on evaluating dissolved contaminant flushing in cylindrical models containing a cylindrical low-conductivity zone (i.e., low-K zone) embedded in a medium with high conductivity. Here seven different porous media, including the four high-conductivity-contrast (SL, SS, LL, and LS), one medium-contrast (LLM), one low-contrast (LLL), and one homogeneous (H) models, were used to analyze the effect of geometry of the low-K zone, K contrast, and flow regime on solute flushing. First, we validated our experiments by comparing the breakthrough curve of the homogeneous (H) model obtained from an analytical solution with that of the experiment. The results of the four high-contrast models showed that for the diffusion-dominated regime, the PVI required to flush out the solute mass is much less than that for the advection-dominated regime. This is because for advection-dominated regimes, the solute is released from the downstream face of the low-K zone via

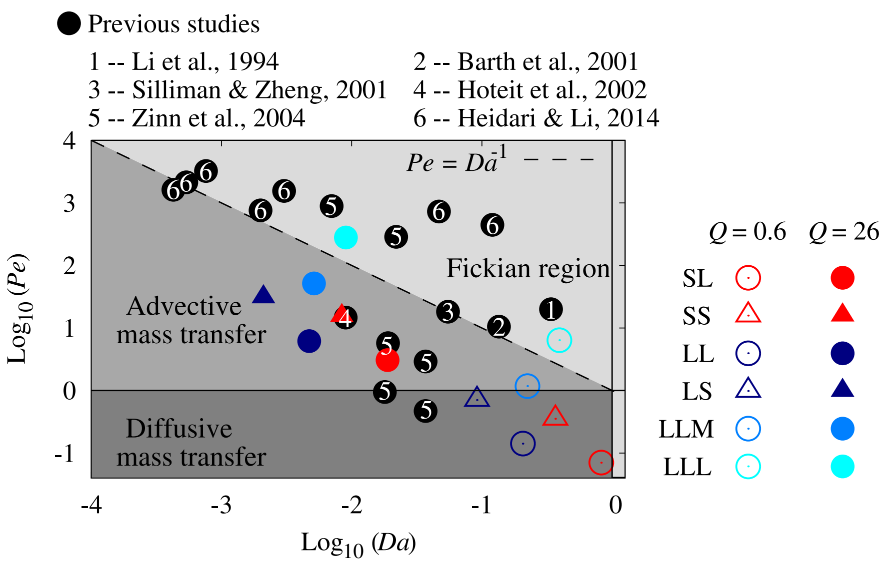

Fig. 11 Representation of the flow regimes in our work compared with those in previous studies

only advection. However, in the case of diffusion-dominated regimes, the solute is removed from all the surfaces via diffusion and from the downstream face via slow advection. Thus, we provided experimental evidence that for diffusion-dominated regimes, the dimensionless time (i.e., PVI) required to flush out the solute is drastically low, as reported by Di Palma et al. (2017), who numerically evaluated solute flushing in low-K zones. Further, to evaluate the pore volumes required to flush out solutes for the four high-contrast models, we introduced a parameter $P_{0.01}$, which is defined as the PVI needed for the relative concentration to become 0.01 at the sensor position. As a result, the value of $P_{0.01}$ monotonically decreases with increasing the specific surface area of the low-K zone for diffusion-dominated regimes, whereas it increases with increasing the length of the low-K zone for advection-dominated regimes. Furthermore, we compared the breakthrough curves of three different models of K contrast (LL, LLM, and LLL). Notably, there exists a distinct difference between the PVI values required to flush out solutes for LLM and LLL, indicating the importance of the effect of K contrast on solute flushing processes. Finally, by comparing the Pe and Da numbers determined in this study and previous experiments, we found that our work has a unique dataset that covers three different regimes (Fickian, advection, and diffusion regimes).

In this work, we focused on volume and aspect ratios as the geometric properties of cylindrical low-K zones; however, the orientations and shapes (i.e., ellipse, rectangular solid, and more complex shapes) of low-K zones would also be controlling factors in the solute flushing process. Therefore, future work should evaluate the effect of such factors.

Acknowledgements This work was supported by JSPS KAKENHI Grant Number JP20J10801, 19H03074, and JP22K20602.

Funding Open access funding provided by Kobe University.

Data Availability The datasets generated and analyzed in the current study are available from the corresponding author on reasonable request.

Declarations

Competing Interests The authors declare no competing interests.

References

Abdoulhalik, A., & Ahmed, A. A. (2017). How does layered heterogeneity affect the ability of subsurface dams to clean up coastal aquifers contaminated with seawater intrusion? *Journal of Hydrology, 553*, 708–721. https://doi.org/10.1016/j.jhydrol.2017.08.044

Appelo, C. A. J., & Postma, D. (2010). *Geochemistry, Groundwater and Pollution* (2nd ed.). CRC Press.

Barth, G. R. M., Hill, M. C., Illangasekare, T. H., & Rajaram, H. (2001). Predictive modeling of flow and transport in a two-dimensional intermediate-scale, heterogeneous porous medium. *Water Resources Research, 37*(10), 2503–2512. https://doi.org/10.1029/2001WR000242

Bear, J. (1972). *Dynamics of fluids in porous media*. Elsevier.

Blue, J., Boving, T., Tuccillo, M. E., Koplos, J., Rose, J., Brooks, M., & Burden, D. (2023). Contaminant back diffusion from low-conductivity matrices: Case studies of remedial strategies. *Water, 15*(3), 570. https://doi.org/10.3390/w15030570

Brooks, M. C., Yarney, E., & Huang, J. (2020). Strategies for managing risk due to back diffusion. *Groundwater Monitoring and Remediation, 41*(1), 76–98. https://doi.org/10.1111/gwmr.12423

Brusseau, M. L., & Guo, Z. (2014). Assessing contaminant-removal conditions and plume persistence through analysis of data from long-term pump-and-treat operations. *Journal of Contaminant Hydrology, 164*, 16–24. https://doi.org/10.1016/j.jconhyd.2014.05.004

Castro-Alcalá, E., Fernàndez-Garcia, D., Carrera, J., & Bolster, D. (2012). Visualization of mixing processes in a heterogeneous sand box aquifer. *Environmental Science and Technology, 46*(6), 3228–3235. https://doi.org/10.1021/es201779p

Chapman, S. W., & Parker, B. L. (2005). Plume persistence due to aquitard back diffusion following dense nonaqueous phase liquid source removal or isolation. *Water Resources Research, 41*(12), W12411. https://doi.org/10.1029/2005WR004224

Chapman, S. W., Parker, B. L., Sale, T. C., & Doner, L. A. (2012). Testing high resolution numerical models for analysis of contaminant storage and release from low permeability zones. *Journal of Contaminant Hydrology, 136–137*, 106–116. https://doi.org/10.1016/j.jconhyd.2012.04.006

Citarella, D., Cupola, F., Tanda, M. G., & Zanini, A. (2015). Evaluation of dispersivity coefficients by means of a laboratory image analysis. *Journal of Contaminant Hydrology, 172*, 10–23. https://doi.org/10.1016/j.jconhyd.2014.11.001

Di Palma, P. R., Parmigiani, A., Huber, C., Guyennon, N., & Viotti, P. (2017). Pore-scale simulations of concentration tails in heterogeneous porous media. *Journal of Contaminant Hydrology, 205*, 47–56. https://doi.org/10.1016/j.jconhyd.2017.08.003

Guswa, A. J., & Freyberg, D. L. (2000). Slow advection and diffusion through low permeability inclusions. *Journal of Contaminant Hydrology, 46*(3–4), 205–232. https://doi.org/10.1016/S0169-7722(00)00136-4

Heidari, P., & Li, L. (2014). Solute transport in low-heterogeneity sandboxes: The role of correlation length and permeability variance. *Water Resources Research, 50*(310), 8240–8264. https://doi.org/10.1002/2013WR014654

Hoteit, H., Mose, R., Younes, A., Lehmann, F., & Ackerer, Ph. (2002). Three-dimensional modeling of mass transfer in porous media using the mixed hybrid finite elements and the random-walk methods. *Mathematical Geology, 34*(4), 435–456. https://doi.org/10.1023/A:1015083111971

Jaeger, S., Ehni, M., Eberhardt, C., Rolle, M., Grathwohl, P., & Gauglitz, G. (2009). CCD camera image analysis for mapping solute concentrations in saturated porous media. *Analytical and Bioanalytical Chemistry, 395*(6), 1867–1876. https://doi.org/10.1007/s00216-009-2978-3

Kurasawa, T., Suzuki, M., & Inoue, K. (2020). Experimental assessment of solute dispersion in stratified porous media. *Hydrological Research Letters, 14*(4), 123–129. https://doi.org/10.3178/hrl.14.123

Kurasawa, T., Takahashi, Y., Suzuki, M., & Inoue, K. (2022). Truncation effect on estimation of transport parameters for slug-injection tracer tests. *Environmental Earth Sciences, 81*(6), 185. https://doi.org/10.1007/s12665-022-10309-9

Li, L., Barry, D. A., Culligan-Hensley, P. J., & Bajracharya, K. (1994). Mass transfer in soils with local stratification of hydraulic conductivity. *Water Resources Research, 30*(11), 2891–2900. https://doi.org/10.1029/94WR01218

McNeil, J. D., Oldenborger, G. A., & Schincariol, R. A. (2006). Quantitative imaging of contaminant distributions in heterogeneous porous media laboratory experiments. *Journal of Contaminant Hydrology, 84*(1–2), 36–54. https://doi.org/10.1016/j.jconhyd.2005.12.005

Parker, B. L., Cherry, J. A., & Chapman, S. W. (2004). Field study of TCE diffusion profiles below DNAPL to assess aquitard integrity. *Journal of Contaminant Hydrology, 74*(1–4), 197–230. https://doi.org/10.1016/j.jconhyd.2004.02.011

Parker, B. L., Chapman, S. W., & Guilbeault, M. A. (2008). Plume persistence caused by back diffusion from thin clay layers in a sand aquifer following TCE source-zone hydraulic isolation. *Journal of Contaminant Hydrology, 102*(1–2), 86–104. https://doi.org/10.1016/j.jconhyd.2008.07.003

Silliman, S. E., & Zheng, L. (2001). Comparison of observations from a laboratory model with stochastic theory: Initial analysis of hydraulic and tracer experiments. *Transport in Porous Media, 42*(1/2), 85–107. https://doi.org/10.1023/A:1006700111701

Tatti, F., Papini, M. P., Raboni, M., & Viotti, P. (2016). Image analysis procedure for studying Back-Diffusion phenomena from low-permeability layers in laboratory tests. *Scientific Reports, 6*, 30400. https://doi.org/10.1038/srep30400

Tatti, F., Papini, M. P., Sappa, G., Raboni, M., Arjmand, F., & Viotti, P. (2018). Contaminant back-diffusion from low-permeability layers as affected by groundwater velocity: A laboratory investigation by box model and image analysis.

Science of the Total Environment, 622–623, 164–171. https://doi.org/10.1016/j.scitotenv.2017.11.347

Tatti, F., Papini, M. P., Torretta, V., Mancini, G., Boni, M. R., & Viotti, P. (2019). Experimental and numerical evaluation of Groundwater Circulation Wells as a remediation technology for persistent, low permeability contaminant source zones. *Journal of Contaminant Hydrology, 222*, 89–100. https://doi.org/10.1016/j.jconhyd.2019.03.001

United States Environmental Protection Agency (2020). Superfund remedy report. 16th edition. EPA.

Yang, M., Annable, M. D., & Jawitz, J. W. (2014). Light reflection visualization to determine solute diffusion into clays. *Journal of Contaminant Hydrology, 161*, 1–9. https://doi.org/10.1016/j.jconhyd.2014.02.007

Yang, M., McCurley, K. L., Annable, M. D., & Jawitz, J. W. (2019). Diffusion of solutes from depleting sources into and out of finite low-permeability zones. *Journal of Contaminant Hydrology, 221*, 127–134. https://doi.org/10.1016/j.jconhyd.2019.01.005

You, X., Liu, S., Dai, C., Guo, Y., Zhong, G., & Duan, Y. (2020). Contaminant occurrence and migration between high- and low-permeability zones in groundwater systems: A review. *Science of the Total Environment, 743*, 140703. https://doi.org/10.1016/j.scitotenv.2020.140703

Zinn, B., Meigs, L. C., Harvey, C. F., Haggerty, R., Peplinski, W. J., & Von Schwerin, C. F. (2004). Experimental visualization of solute transport and mass transfer processes in two-dimensional conductivity fields with connected regions of high conductivity. *Environmental Science and Technology, 38*(14), 3916–3926. https://doi.org/10.1021/es034958g